Chapter 3.5 Cross-Scale Energy Transport in Space Plasmas: Applications to the Magnetopause Boundary

Katariina Nykyri [1], Xuanye Ma [1], Jay Johnson [2]

[1]Center for Space and Atmospheric Research and Physical Sciences Department, Embry-Riddle Aeronautical University, Daytona Beach, FL, USA
[2]Department of Engineering, Andrews University, Berrien Springs, MI, USA

Corresponding author: Katariina Nykyri, nykyrik@erau.edu

Abstract

As space plasmas are highly collisionless and involve several temporal and spatial scales, understanding the physical mechanisms responsible for energy transport between these scales is a challenge. Ideally, to study cross-scale space plasma processes, simultaneous multi-spacecraft measurements in three different scales (fluid, ion and electron) would be required together with adequate instrumental temporal resolution. In this chapter we discuss cross-scale energy transport mechanisms mainly focusing on velocity shear driven Kelvin-Helmholtz instability and resulting secondary instabilities and processes, e.g, magnetic reconnection, kinetic magnetosonic waves and kinetic Alfvén waves/mode conversion.

1 Introduction

Unlike regular fluids space plasmas are highly collisionless and involve different length scales which makes understanding the physical mechanisms responsible for energy transport between these scales a challenge. For example, the free mean path between collisions in the solar wind is about 1 AU, making them very rare. Despite of the nearly collisionless nature of the solar wind plasma a standing shock wave, the bow shock, is formed about 14 R_E from the Earth when the magnetized solar wind approaches Earth's magnetic field. Like in a collisional medium, this shock decelerates and heats the solar wind flow. The region between bow shock and magnetopause is called the magnetosheath and consists of shocked solar wind flow characterized by fluctuations in velocity, magnetic field and density. Despite the deceleration of the solar wind at the bow shock there still exists a substantial velocity shear at the magnetopause boundary, with shear increasing gradually from the subsolar magnetopause toward the flanks. Beyond the dawn-dusk terminator the velocity shear is of the order of the solar wind speed. When moving through the velocity shear layer at the flanks into the tail magnetosphere the plasma flow reduces, plasma temperature increases by $\approx$ factor of 50 and specific entropy, which is a measure of non-adiabatic processes (heating and/or diffusion), increases nearly by two orders of magnitude [*Borovsky and Cayton*, 2011]. Furthermore, it has been shown that the ion to electron temperature ratio, T_i/T_e, varies from from 4 to 12 in the magnetosheath and from 2 to 12 in the tail plasma sheet [*Wang et al.*, 2012]. This suggests that the non-adiabatic heating associated with the entry mechanism enhances both the ion and electron temperatures almost by the same proportion. Note that the typical velocity shear layer thickness is about one to two orders of magnitude larger than the ion inertial length, $d_i = c/\omega_{pi} \approx 50-150\,\text{km}$ in the vicinity of the flank magnetopause where c is the speed of light and ω_{pi} is the ion plasma frequency. Therefore, the energy conversion from solar wind bulk flow kinetic energy into the thermal energy of the magnetotail plasma sheet particles occurs in "cross the scale" fashion.

Figure 1a shows a time-scale vs spatial scale graph of the scale sizes occurring in space plasmas with some example processes, starting at each scale. The largest scale is the magnetohydrodynamic (MHD) scale, which describes the plasma systems with slow ($\Delta t \ll 1/f_{ic}$) temporal scales and large ($k \ll 2\pi/d_i$) spatial scales. Here Δt is the process duration, f_{ic} is the ion cyclotron frequency, and k is the wave number. Equation 1 shows the total current transport equation, the generalized Ohm's law. For ideal MHD, plasma is frozen to the magnetic field and the right hand side of Equation 1 is zero. The terms on the right-hand side are the electron inertial term, electron pressure term, Hall-term and resistivity term, respectively.

$$\mathbf{E} + \mathbf{u} \times \mathbf{B} = \frac{m_e m_i}{e^2 \rho} \left[\frac{\partial \mathbf{j}}{\partial t} + \nabla \cdot (\mathbf{uj} + \mathbf{ju}) \right] - \frac{M}{e\rho} \nabla \cdot \mathbf{P_e} + \frac{\mathbf{m_i}}{\mathbf{e}\rho} \mathbf{j} \times \mathbf{B} + \eta \mathbf{j} \tag{1}$$

Here $\mathbf{E}, \mathbf{u}, \mathbf{B}, \mathbf{j}$ are the electric field, plasma bulk velocity, magnetic field, and current density, respectively. M, m_i, m_e, ρ, e denote the total mass, ion mass, electron mass, plasma mass density, and electron charge. Electron pressure tensor is $\mathbf{P_e}$, and plasma resistivity is η. In physical systems, wave particle interactions can act like collisions and mimic effective resistivity. The main contribution to the electric field in MHD scale is provided by the convection electric field. The next scale is the ion inertial scale below which ions can become de-magnetized. The Hall-term and electron pressure term scale as the ion inertial length. The ion-electron hybrid scale involve full kinetic ion physics e.g, finite larmor radius effects but the electron fluid is still frozen to the magnetic field. Electrons can be de-magnetized by processes that act on electron inertial or electron gyro-radius scale. The electron inertial term scales as electron inertial length squared, and resistivity term scales as magnetic Reynolds number.

Up to now the multi-spacecraft space missions such as Cluster, THEMIS, and MMS have covered 3-D measurements on a single scale as at least four spacecraft are required for calculation of gradients, curls and vorticities. Therefore, numerical simulations using different plasma approximations have been invaluable for providing information of the missing scale and for putting spacecraft measurements into context.

In this chapter we discuss cross-scale energy transport mechanisms focusing on velocity shear driven Kelvin-Helmholtz (KH) instability and resulting secondary instabilities, processes and energy transfer mainly from fluid to the ion scales.

1.1 Kelvin-Helmholtz Instability

The interface between two fluids moving with different velocity can be unstable to the Kelvin-Helmholtz instability (KHI). The free energy for the KHI is the kinetic energy that becomes available due to the velocity shear of anti-parallel velocity components across a plane boundary. A non-viscous fluid is always KH unstable in the presence of the velocity shear across an infinitely thin boundary, and its growth rate, for a simple case with uniform density, is $q = kV_0/2$, where V_0 is the difference of the velocities across the shear flow layer and $k = 2\pi/\lambda$ is the wave number. This indicates that short wave lengths (small λ) grow fastest, and that large velocity shear increases the growth rate. Fluid Kelvin-Helmholtz vortices can be seen often when a velocity shear is present: e.g, in merging of two rivers.

The onset condition for the KH mode in an ideal, incompressible plasma with a discontinuous (arbitrarily thin) velocity shear layer is

$$\frac{m_0 n_1 n_2}{n_1 + n_2} [\mathbf{k} \cdot \Delta\mathbf{V}]^2 > \frac{1}{\mu_0} \left[(\mathbf{k} \cdot \mathbf{B}_1)^2 + (\mathbf{k} \cdot \mathbf{B}_2)^2 \right] \tag{2}$$

[*Chandrasekhar*, 1961], where m_0 is the ion mass, n is number density, $\Delta\mathbf{V} = (\mathbf{V}_1 - \mathbf{V}_2)$ is the velocity shear, $\mathbf{B}$ is the magnetic field vector, and the indices denote plasma properties on the two sides of the boundary. One can see that the KHI is stabilized for large magnetic field values along the k-vector of the instability. A finite thickness of the shear layer stabilizes the KH mode for small wavelengths. Also, compressibility ($\nabla \cdot \mathbf{V} \neq \mathbf{0}$) of plasma has a stabilizing effect on KH mode [*Miura and Pritchett*, 1982].

The KHI has been observed by in-situ spacecraft measurements at the Earth's magnetopause during southward IMF [*Hwang et al.*, 2011a; *Yan et al.*, 2014], northward [*Fairfield et al.*, 2000; *Hasegawa et al.*, 2004; *Lin et al.*, 2014; *Eriksson et al.*, 2016] and Parker Spiral (PS) IMF [*Nykyri et al.*, 2006; *Moore*, 2012; *Moore et al.*, 2016]. It has also been observed at the boundary layers of other planets (e.g., *Masson and Nykyri* [2018]; *Johnson et al.* [2014] and references therein) as well as at the boundary of the CMEs [*Foullon et al.*, 2011, 2013; *Nykyri and Foullon*, 2013].

A statistical study using data from NASA's THEMIS mission between 2007-2013 has shown that KH waves are frequent at the magnetopause, occurring about 19 per-

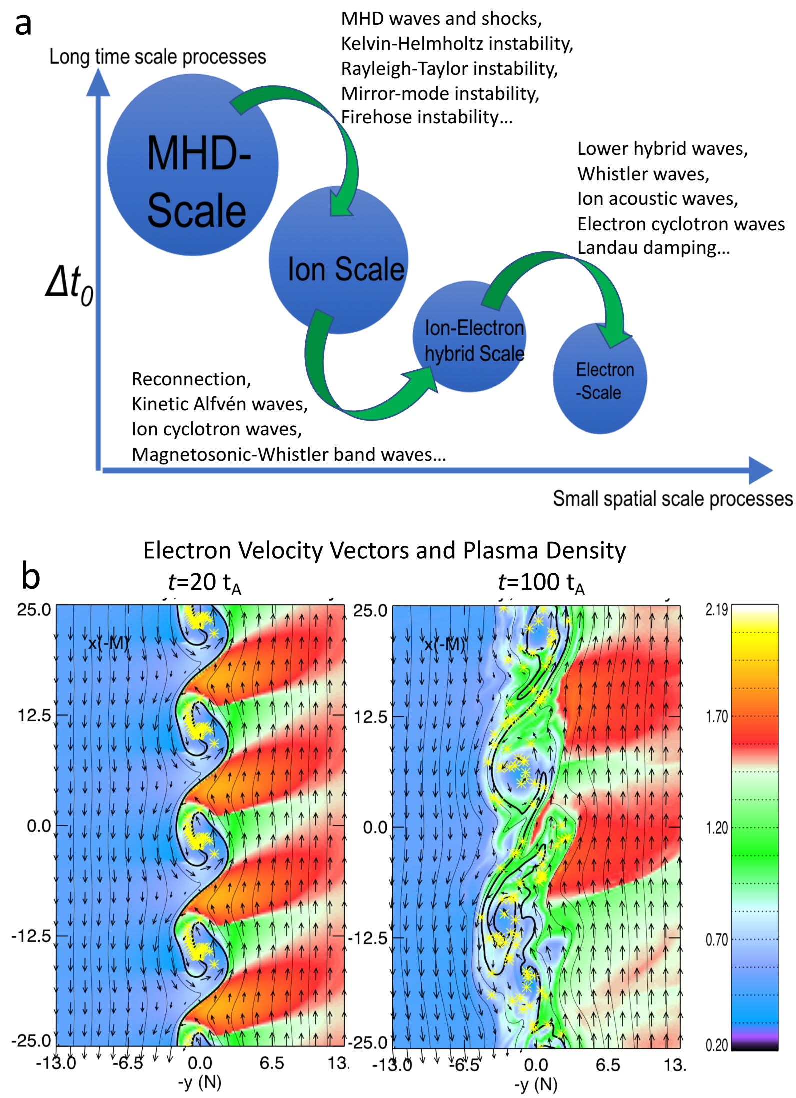

Figure 1. A pictogram presenting time vs size graph of the typical time and length scales occurring in space plasmas. The transport of energy, mass and momentum occurs via "cross-scale" physical processes. The electron velocity (arrows) and plasma number density (color) from a 2-D Hall-MHD simulation at $t = 20$ and 100 Alfvén time in panel (a) and (b), respectively.

cent of the time during all magnetopause crossings [*Kavosi and Raeder*, 2015]. *Henry et al.* [2017] showed that KHI occurrence rate shows a strong preference toward the dawn magnetopause for PS IMF and a strong preference toward the dusk is observed for northward IMF. However, the KH event at the dusk are observed for higher solar wind speeds. The dawn preference for the PS orientation can be explained both by smaller magnetic field tension at the dawn-dusk terminator for the PS IMF orientation [*Nykyri*, 2013] and by enhanced amount of low frequency, high-amplitude velocity field fluctuations existing at the dawn magnetosheath [*Nykyri and Dimmock*, 2016; *Nykyri et al.*, 2017] driven by fore-shock processes.

One of the important feature of the KH instability is that it can form small scale structure in its nonlinear stage.

1.2 Magnetic Reconnection

Magnetic reconnection requires an existence of a magnetic shear across a thin current sheet, where kinetic processes can break the frozen-in condition (see e.g, *Biskamp* [2000] and Chapter 2.1). One such process is the tearing instability, which can lead to a reconnection in its non-linear stage [*Chen et al.*, 1997]. The MMS spacecraft were designed to unravel the micro-physics of magnetic reconnection and just seven months after launch the spacecraft encountered the electron diffusion region for the first time [*Burch et al.*, 2016]. The 3D plasma measurements, that were made 100 times faster than in any previous missions, revealed that the primary source of the reconnection electric field is the divergence of the electron pressure tensor and that crescent-shaped electron velocity distributions carry the out-of-plane current. The reconnection was shown mostly to be laminar near the X-line with wave generation and turbulence becoming important in adjacent regions [*Graham et al.*, 2017]. MMS observations also revealed that electron heating in the ion diffusion region of magnetic reconnection is consistent with large-scale parallel electric fields, which trap and accelerate electrons, rather than wave-particle interactions [*Graham et al.*, 2016].

In addition, the processes taking place within the bow shock and magnetosheath also affect the boundary conditions for reconnection onset. THEMIS spacecraft showed that magnetosheath jets, localized 1-2 R_E bursts of high dynamic pressure, compressed the originally thick (60 - 70 d_i), high magnetic shear magnetopause until it was thin enough for reconnection to occur [*Hietala et al.*, 2018]. Also, mirror mode waves (see e.g., *Dimmock et al.* [2015] and references therein), generated by the ion temperature asymmetry in the magnetosheath can affect magnetopause reconnection rate [*Laitinen et al.*, 2010].

One of the critical questions related to reconnection onset is understanding how the thin current sheets are generated.

2 Magnetic Reconnection and KHI

2.1 2-D geometry

Relative configuration of velocity shear and magnetic shear determines the nonlinear interaction between the KHI and magnetic reconnection. A large shear flow aligned with a large magnetic shear appears to be the simplest 2-D configuration that favors for both magnetic reconnection and the KHI. Tearing mode dominates current sheet evolution for sub-Alfvénic flows, while KHI unstable regime can occur for super Alfvénic flows (see e.g, *Chen et al.* [1997] and reference therein).

The magnetic field component that is strictly perpendicular to the KH wave vector does not influence the whole processes. Nevertheless, magnetic reconnection can be trigged as a secondary instability if there is a small magnetic field component along the KH wave-vector direction [*Otto and Fairfield*, 2000; *Fairfield et al.*, 2000]. In the nonlinear stage of the KHI, the well developed KH vortex will twist magnetic field lines, thereby forming a thin current layer [*Nykyri and Otto*, 2001, 2004]. Magnetic reconnection can therefore operate if the the width of the current layer is comparable to the ion inertia scale [*Hasegawa et al.*, 2009]. Figure 1b shows an example of the 2-D Hall-MHD simulation of the electron velocity and plasma number density. By $t = 20$ Alfvén times (t_A) four KH vortices are visible and $80t_A$ later vortices have coalesced into larger vortices due to magnetic reconnection occurring in thin current sheets with thickness of the order of ion inertial length.

In principle there are two types of 2-D KHI driven magnetic reconnection [*Nakamura et al.*, 2006; *Nakamura et al.*, 2008] (see also Chapter 3.5). Type I occurs for the initial antiparallel in-plane magnetic field components, in which magnetic reconnection connect the magnetic field from both sides of the boundary layer. Meanwhile, Type II occurs for the initial parallel in-plane magnetic field components. In this case, magnetic reconnection connects the magnetic field from the same side of the boundary layer. In three dimensional configuration, the large perturbation contains the broad wave spectra along the different directions [*Nakamura et al.*, 2017; *Delamere et al.*, 2018]. Thus, both Type I and Type II can operate simultaneously [*Nykyri et al.*, 2006].

MMS spacecraft recorded direct evidence of reconnection exhausts associated with strongly compressed current sheets created by KH waves [*Eriksson et al.*, 2016; *Li et al.*, 2016]].

2.2 3-D geometry

Figure 2 is a sketch of 3-D nonlinear interaction between reconnection and the KHI under northward IMF conditions. The black lines represent the closed magnetospheric field lines, whose footprints at high latitudes connect to the north and south poles. The red lines are the magnetosheath field lines, connecting to the solar wind, which move into a tailward direction. The nonlinear KH wave generates vorticity at low latitudes, which is indicated by green arrows in Figure 2. The strong bending of the magnetic field line generates large antiparallel magnetic field components at middle latitudes, and eventually forms a pair of middle-latitude reconnection sites (cyan cycles in Figure 2). Note that after reconnection ceases to operate, the original magnetosheath (magnetospheric) field line (left panel) between the pair of middle-latitude reconnection sites becomes a magnetospheric (magnetosheath) field line (right panel). This exchanged flux is referred to as “double reconnected flux”. Several MHD simulation studies [*Faganello et al.*, 2012; *Borgogno et al.*, 2015; *Leroy and Keppens*, 2017] show that this process exchanges plasma between the magnetosphere and magnetosheath, being different from the classical diffusion process and the 2-D nonlinear interaction between reconnection and the KHI suggested by *Nykyri and Otto* [2001]. Recently, *Vernisse et al.* [2016] reported a very frequent presence of additional boundary layer signatures, which can be an indication of middle-latitude double reconnection.

It is estimated that the diffusion coefficient associated with this 3-D nonlinear interaction between reconnection and long-wavelength KH modes (i.e., the wavelength is about several Earth radii) at Earth's magnetopause can be greater than $10^{10}\,\mathrm{m^2\,s^{-1}}$ [*Ma et al.*, 2017], which is one order of magnitude greater than the results from the 2-D geometry. However, the scenario sketched in Figure 2 is an idealized configuration with a north-south symmetry assumption. Open flux is expected to be created through asymmetries of the boundary, through interhemispheric asymmetries, and through asymmetries arising from turbulence (stochastic effects). For long-wavelength KH modes the overall double reconnected flux is mostly determined by the KH wave (i.e., sheath-sphere conditions) rather than the specific detail of the reconnection diffusion region once reconnection operates. A large magnetic shear decreases the KH growth rate, and increases the portion of open flux, which significantly reduces the plasma and the flux tube entropy transport efficiency.

A realistic three-dimensional configuration of Earth's magnetospheric flanks for southward IMF conditions includes large anti-parallel magnetic components with a fast perpendicular sheared flow. Both magnetic reconnection and KHI can operate simultaneously [*Hwang et al.*, 2011b; *Yan et al.*, 2014; *Walsh et al.*, 2015]. In the nonlinear stage, both magnetic reconnection and KH modes mutually impact the onset and operating conditions of each other by changing the width of the transition layer, i.e., the current layer and the sheared flow layer. Thus, the normalized magnetic reconnection rate is strongly increased by nonlinear KH waves; however, these waves also limit the total reconnected flux by dissipating the electric current when the largest wavelength

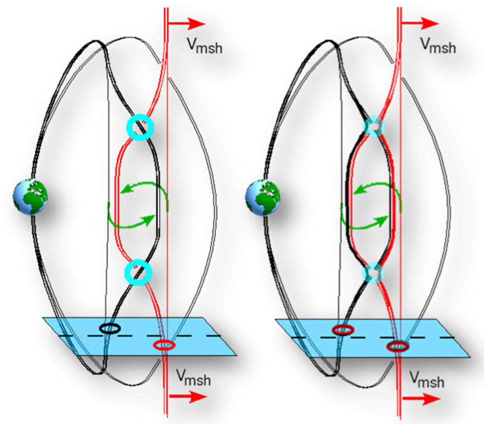

Figure 2. Sketch of the 3-D nonlinear interaction between reconnection and the KHI under northward IMF conditions. The black and red lines are represented for the closed magnetospheric field line and solar wind field line before (left) and after (right) middle-latitude double reconnection operates, respectively. The cyan circles highlight the middle-latitude reconnection sites [*Ma et al.*, 2017].

mode becomes highly nonlinear. This is particularly remarkable because the interaction leads to fast reconnection with local rates that are equal to the Petschek rate of fast reconnection without invoking Hall physics. It has also been demonstrated that the diffusion region and the distribution of field-aligned currents are strongly modified by the KH waves [*Ma et al.*, 2014a,b].

The KHI can be stabilized by a super fast shear flow, that flow jump is greater than the local fast mode speed [*Miura and Kan*, 1992]. A scaling analysis implies a contradiction between the Walén relation and the balance of the total pressure for magnetic reconnection with such a fast perpendicular sheared flow. It is demonstrated that the reconnection layer violates the Walén relation but still maintains the total pressure balance in such a configuration [*Ma et al.*, 2016]. The results show an expanded outflow region, consistent with the presence of divergent normal flow, and a significant decrease of the plasma density as well as the thermal pressure in the outflow region. Nevertheless, the quasi-steady reconnection rate remains of order 0.1 [*Liu et al.*, 2018] in this configuration.

3 From MHD Scales to Kinetic Scales

The non-linear development of the KHI can lead to creation of thin current layers, where secondary instabilities and ion and electron scale processes can operate.

3.1 Non-linear Development of the KHI: Vortex Structures, Coalescence, and Secondary Instabilities

The vortex structure in the nonlinear stage of KH instability can transport the plasma cross the flow shear. Such vortices are commonly seen in MHD and Hall-MHD simulations [*Miura*, 1987; *Otto and Fairfield*, 2000; *Nykyri and Otto*, 2004] (see Figure 1b) and particle simulations [*Thomas and Winske*, 1993; *Fujimoto and Terasawa*, 1994; *Wilber and Winglee*, 1995; *Matsumoto and Hoshino*, 2004; *Nakamura et al.*, 2011; *Cowee et al.*, 2009; *Delamere et al.*, 2011] of the KHI. Typically, small-scale vortices saturate at smaller amplitude than large vortices, and small scale vortices coalesce nonlinearly to form larger-scale vortices leading to an inverse-cascade of wave power [*Winant and Browand*, 1974]. The 2D nonlinear ideal MHD study of *Miura* [1997] showed that growth of the longer wave length modes (subharmonics) tends to occur on a timescale comparable to their linear growth rate suggestive that the emergence of larger scale vortices is due to the linear growth of the subharmonic modes. However, the 2D MHD and PIC simulations of *Matsumoto and Seki* [2010] suggested a substantially larger growth of subharmonics occurs when a broad spectrum of subharmonics is included. These processes rapidly broaden the boundary layer and transfer mass, momentum, and energy across the boundary.

The formation of vortices can also lead to secondary instabilities (secondary KH and Rayleigh Taylor (RT)) driven by the centrifugal force of the rotating fluid, leading to a broad mixing layer when ion inertia/gyroradius effects allow ions to move across magnetic field [*Thomas and Winske*, 1993; *Nakamura et al.*, 2004; *Matsumoto and Hoshino*, 2006; *Cowee et al.*, 2009; *Delamere et al.*, 2011; *Nakamura and Daughton*, 2014].

Matsumoto and Hoshino [2006] performed full particle simulations of KH (with no magnetic shear) and found fast turbulent mixing and transport when there exist a density difference across the interface. The turbulence is triggered by secondary KH and RT instabilities. The strong electrostatic field caused by the secondary RT instability scatters ions and deforms the electron density interface. They also showed that asymmetric density across the shear flow boundary increases the mixing area rate by 2 to 4 times faster compared to the symmetric density case.

Cowee et al. [2009] also used two-dimensional hybrid simulations to examine transport across the magnetopause (flow perpendicular to the field). Particles were tracked during the simulation to determine how they are transported. The diffusion coefficients were time dependent with a probability distribution of jump lengths that was non-Gaussian leading to an enhancement of mixing over the classical diffusion limit, which therefore is referred as to “super diffusion” by *Cowee et al.* [2009]. They also found that the collapse of vortices form small-scale turbulence, increasing the diffusion coefficient, which, however, is ultimately controlled by the growth of large-scale vortices. *Delamere et al.* [2011] also demonstrated the role of mixing as the vortices evolve, and found that heavy ions (i.e., OH^+) suppress the growth of modes with wavelengths greater than the ion inertial length (larger for heavier ions), which reduces the overall growth and mixing associated with the instability. Momentum transport across the magnetopause will significantly affect flows in the boundary layer and generate tailward flows along the dawn flank.

Two-dimensional MHD simulations [*Matsumoto and Seki*, 2010] of the KHI with transverse magnetic field and highly asymmetric density configurations in a large simulation domain show that rapid formation of a broad plasma turbulent layer can be achieved by forward and inverse energy cascades of the KHI. The forward cascade is triggered by growth of the secondary RT instability excited during the nonlinear evolution of the KHI and forms smaller scale structures than the KH mode (but is still above ion inertial scale as these are MHD simulations). The inverse cascade to longer wave lengths is accomplished by nonlinear mode couplings between the fastest growing mode of the KHI and other KH unstable modes. While two-dimensional simulations typically show suppression of the secondary instabilities when magnetic shear is present, more recent three-dimensional kinetic simulations suggest that secondary instabilities will develop in regions where $\mathbf{k} \cdot \mathbf{B} = 0$ leading to sub ion-inertial scale structures, and enhanced mixing and transport [*Nakamura and Daughton*, 2014].

Furthermore, high resolution global hybrid simulations of the magnetosheath have demonstrated that ion scale fore-shock driven processes can develop complicated structures (e.g., jets, flux ropes, waves and turbulence) in the magnetosheath and can impact the magnetopause dynamics [*Karimabadi et al.*, 2014].

3.2 Cross-scale coupling from MHD scale waves to kinetic scale waves at the magnetopause

3.2.1 Kinetic Alfvén Waves

Kinetic Alfvén waves (KAW) are Alfvénic fluctuations with spatial scales the order of the ion gyroradius. At these scales, ions no longer move together with field lines because the ion polarization drift is significant compared with the $\mathbf{E}\times\mathbf{B}$ velocity. Because the electrons must remain on the field lines, parallel electric fields develop to maintain charge neutrality. These parallel electric fields can accelerate electrons [*Hasegawa and Chen*, 1976; *Chaston et al.*, 2007a]. At these scales, the large amplitude waves detected near the magnetopause can also effectively interact with ions through a nonlinear resonance between the polarization drift and gyromotion [*Stasiewicz et al.*, 2000; *Johnson and Cheng*, 2001; *Chen et al.*, 2001; *Chaston et al.*, 2014] leading to significant perpendicular ion heating and transport [*Johnson and Wing*, 2009a].

Mode conversion is one process that generates KAWs [*Hasegawa and Chen*, 1976; *Lee et al.*, 1994; *Johnson and Cheng*, 1997; *Chaston et al.*, 2007]. It occurs when compressional Alfvén waves propagate to a resonant field line where wave energy accumulates at the Alfvén resonance location ($\omega = k_{\|}v_A$) and slowly radiates away as a KAWs having gyroradius scale. Mode conversion is particularly important in a region having large gradient in the Alfvén velocity such as the magnetopause. KAWs are also generated near reconnection sites leading to plasma heating in the reconnection exhaust [*Chaston et al.*, 2009; *Vaivads et al.*, 2010; *Shay et al.*, 2011; *Liang et al.*, 2016, 2017; *Dai et al.*, 2017]. Velocity shear is another source of free energy that can lead to direct generation of Alfvén waves when the sheared flow layer is in close proximity to Alfvén velocity gradients [*Taroyan and Erdelyi*, 2002]. Velocity shear also lead to indirect generation of KAWs through the development of nonlinear Kelvin-Helmholtz vortex structures with sharp gradients in the Alfvén velocity [*Chaston et al.*, 2007], which facilitate the mode conversion process described above.

The importance of KAW driven transport has been inferred from estimates of diffusion coefficients based on wave properties observed at the magnetopause [*Hasegawa and Mima*, 1978; *Lee et al.*, 1994; *Johnson and Cheng*, 1997; *Chaston et al.*, 2007, 2008; *Izutsu et al.*, 2012]. Although direct observations of plasma entry with diffusion drift speed the order of 1 km/s is not possible with present day instrumentation, there is considerable evidence for KAW induced transport based on observations of plasma populations near the magnetopause. For instance, statistical surveys of plasma populations near the magnetopause exhibit properties that are expected from KAWs such as the correlation between the distribution of KAWs along the magnetopause and the entry of magnetosheath plasma into the magnetosphere [*Wing et al.*, 2005; *Yao et al.*, 2011]. Specific features of the velocity space distributions of the transported ions are also consistent with KAW interactions [*Izutsu et al.*, 2012; *Chaston et al.*, 2013].

Observations from multi-spacecraft missions in the magnetosphere have made it possible to identify some of the broadband wave activity across the magnetopause as KAWs. Measurements of the scale of these waves has been used to make robust estimates of the transport rates that these waves can drive. Based on the amplitudes of wave observations *Chaston et al.* [2008] estimated the diffusion coefficient to be the order of $5\times10^9\mathrm{m}^2/\mathrm{s}$ as required to populate the low latitude boundary layer [*Sonnerup*, 1980].

Asymmetries in the observed spectra at the magnetopause [*Yao et al.*, 2011] are consistent with observations of dawn-dusk asymmetry in plasma sheet populations near the flanks [*Wing et al.*, 2005]. *Chaston et al.* [2013] also found observational evidence that KAWs can rapidly heat ions at 1eV/s when the wave amplitude exceeds a threshold as proposed by [*Johnson and Cheng*, 2001]. *Izutsu et al.* [2012] noted that because transport in KAWs is energy dependent, it should be possible to see an energy dependence in the transport of plasma across the magnetopause by comparing distribution functions. To interact with the waves, the particles must be in resonance with the waves, which selectively transports more energetic particles. One feature of the observations of cold dense plasma material [*Wing et al.*, 2005; *Johnson and Wing*, 2009b] is that the temperature increases across the flanks, which could be the result of such a filtering effect.

Recent global hybrid simulations have demonstrated that mode conversion occurs at the magnetopause [*Shi et al.*, 2013]. The KAWs seen in the simulation satisfy the correct dispersion relation and the spectrum of $\delta\mathbf{E}/\delta\mathbf{B}$ is consistent with KAWs. 3D local simulations have also demonstrated how a two-step process consisting of linear mode conversion followed by parametric decay can lead to the wave spectra required for efficient transport [*Lin et al.*, 2012].

It has also been recognized that KAWs can play an important role in magnetic reconnection. KAWs have been observed near X-lines [*Chaston et al.*, 2005] with sufficient amplitude to account for plasma transport in the diffusion region [*Chaston et al.*, 2009]. *Vaivads et al.* [2010] identified KAWs near the boundary of the reconnection jet in regions of sharp gradient in the Alfvén velocity (the Alfvén edge), while *Shay et al.* [2011] showed that a significant Poynting flux of KAWs radiates away from the X-line in particle simulations. A recent hybrid simulation has shown that KAWs originate near the X-line [*Liang et al.*, 2016] and interact with ions through nonlinear Landau damping and stochastic heating in the exhaust region [*Liang et al.*, 2017].

Velocity shear can also facilitate the generation of KAWs in two ways: directly and indirectly. Direct generation occurs when the free energy in the shear flow layer drives an instability that couples the shear layer with a resonant Alfvén wave [*Taroyan and Erdelyi*, 2002]. The energy transfer is facilitated by a compressional wave that transfers energy from the flow shear region to a nearby field line that resonates with the wave. In the flow region, there are forward and backward propagating stable K-H waves. When the real frequency of the KH mode lies within the frequency range of resonant field lines (known as the Alfvén continuum) there can be positive or negative feedback leading to growth or damping. The Doppler shifted backward propagating mode becomes unstable and couples with the positive band of the Alfvén continuum. This instability occurs with a lower threshold than the typical KH instability and leads to the growth of a resonant Alfvén wave. As in mode conversion, the resonance is resolved by kinetic effects and the energy slowly radiates away as a kinetic Alfvén wave.

The velocity shear can also facilitate KAW development in the boundary layer indirectly through the nonlinear development of KH vortices. Due to large changes in density and magnetic within a KH structure, the Alfvén velocity profile across the vortices develops large variation in the Alfvén speed, which leads to the formation of deep Alfvén velocity minima (wells). The mode conversion process can then trap KAWs in the edge of the wells leading to transport and heating as described above [*Chaston et al.*, 2007].

3.2.2 Magnetosonic Waves

Using data from two Cluster spacecraft 80 km apart *Moore et al.* [2016] were able to identify an ion-scale (200-2000 km) magnetosonic wave packet inside KH vortex by derivation of the experimental dispersion relation. The vortex region was characterized by total pressure minimum and existence of fluid-scale KHI was determined by compar-

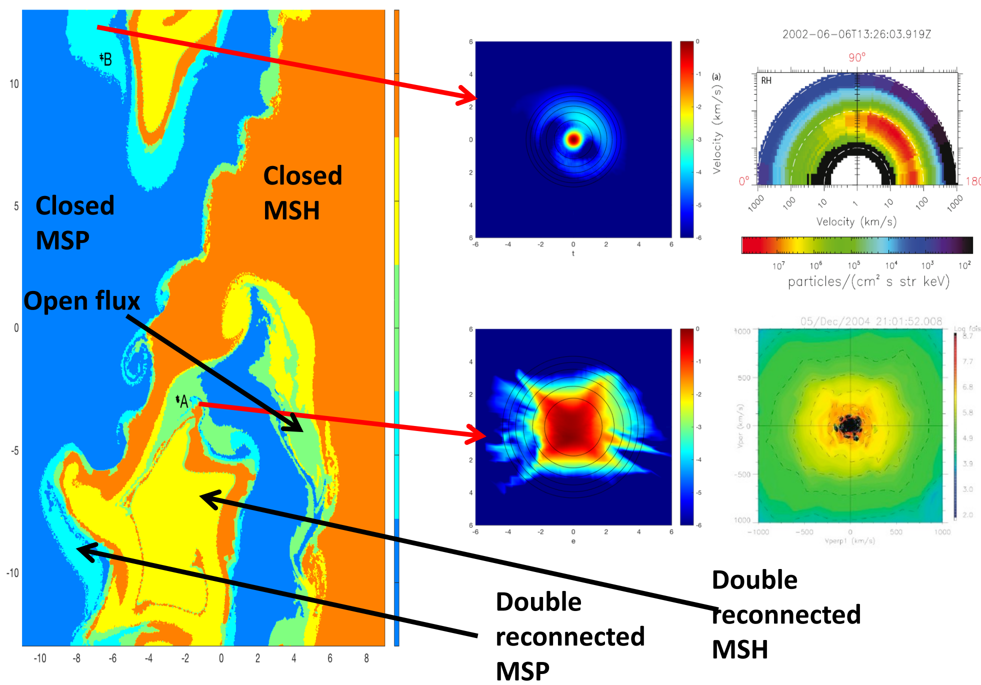

Figure 3. Test particle velocity distribution functions (middle) in 3-D MHD simulation (left) observed at the regions of different magnetic field topologies generated by the magnetic reconnection during KHI. On right are examples of the velocity distribution functions (shell [*Moore et al.*, 2016] and diamond [*Taylor and Lavraud*, 2008]) observed by Cluster and Double Star spacecraft during KHI, respectively.

ing Cluster data with MHD simulations. The experimental dispersion curve matched very well the theoretical dispersion relation of the MHD Fast Mode Wave (FMW) $\omega^2 = \frac{k^2}{2}\{c_{ms}^2 + \left[(v_A^2 - c_s^2)^2 + 4v_A^2 c_s^2 \frac{k_\perp^2}{k^2}\right]^{1/2}\}$ as well as the kinetic magnetosonic solution from WHAMP code *[Rönnmark, 1982]*, particularly at higher frequencies and wave numbers. The Poynting flux during the wave packet close to the eye of the KH vortex matched the observed $\approx$ 2 keV heating of the ions of magnetosheath origin. Furthermore, waves consistent with KAW properties were identified in magnetosheath side of the vortex. Subsequent statistical study by *Moore et al.* [2017] showed that when KHI is active more obliquely propagating ion scale waves with higher Poynting flux exist in the magnetospheric side of the magnetopause, when compared to boundary crossings without KHI. It was also found that specific entropy during transition from magnetosheath into magnetosphere is more enhanced during KHI. The wave characteristics of the statistical study were consistent with kinetic Alfvén and Magnetosonic -Whistler regimes [*Moore et al.*, 2017]. The free-energy for the magnetosonic wave generation is contained in shell-like ion and electron velocity distributions [*Moore et al.*, 2016]. The ion beam-distributions during reconnection in KH vortices have also been observed [*Nykyri et al.*, 2006]. The fact that these ion scale waves are more abundant during KHI suggests that KH provides more free-energy for the ion-scale wave generation.

Figure 3 shows our initial results of the test particle simulations inside 3-D KH vortex with ongoing magnetic reconnection (similar as sketched in Figure 2) below and above the shear-flow plane. The 3-D reconnection in KH vortices results in complex magnetic field topologies including regions of i) closed magnetospheric and ii) closed magnetosheath flux, iii) open flux, iv) double reconnected magnetosheath, and v) double reconnected magnetospheric flux. A shell like ion velocity distribution function was observed in the region of double reconnected magnetospheric flux similar to Cluster spacecraft observations by *Moore et al.* [2016]. A diamond shaped distribution was observed at the boundary of open flux and closed magnetospheric flux previously observed in Cluster observations during KH event [*Taylor and Lavraud*, 2008].

The MMS KHI event studied by *Eriksson et al.* [2016] also showed presence of turbulent power laws [*Stawarz et al.*, 2016], as well as large-amplitude, parallel, electrostatic waves below ion plasma frequency [*Wilder et al.*, 2016] that were possibly ion acoustic waves. This demonstrates that MHD scale KHI is rich with secondary processes and various kinetic scale wave phenomena.

4 Summary and Discussion

In the present chapter we have discussed cross-scale coupling mechanisms at the Earth's magnetopause boundary pertaining to KHI, magnetic reconnection, wave-particle interactions, and turbulence. Future studies need to address whether lower hybrid waves, such as observed by *Graham et al.* [2017] trigger reconnection or they are simply a consequence of reconnection. Scale analysis based on the pressure balance shows that magnetic reconnection under the typical magnetopause environment alone cannot provide a sufficient macroscale heating source [*Ma and Otto*, 2014], highlighting possible importance of KHI driven cross-scale wave particle interactions [*Johnson and Cheng*, 2001; *Moore et al.*, 2016, 2017] as a viable ion-scale heating mechanism. Further studies are required to demonstrate whether the magnetosonic-whistler branch waves that were shown to provide significant ion heating [*Moore et al.*, 2016] continue to have sufficient power at electron scales to contribute to electron heating, and possibly explain the near-constancy of the ion to electron temperature ratios at the flank magnetopause [*Wang et al.*, 2012]. Recent MMS observations have also revealed how low-latitude component reconnection can lead to formation of diamagnetic cavities at higher latitudes due to particle trapping [*Nykyri et al.*, 2019]. This is similar to mechanism previously observed at the vicinity of high-altitude cusps initiated by anti-parallel reconnection [*Nykyri et al.*, 2011, 2012]. The relative role of various processes in plasma heating and particle acceleration in these cavities remains to be further studied, but unlike heating in diffusion regions, particle energization in these cavities would have a volume filling effect, possibly contributing to the macro-scale magnetospheric heating.

In addition, understanding the cross-scale coupling processes in solar wind-magnetosphere system will be crucial for improving space weather prediction. Therefore, future space missions and computer models should address the problem of cross-scale coupling. This will require development of constellation missions of at least 10 spacecraft spanning simultaneously the fluid, ion and electron scales, as well as developing new numerical codes and data-analysis methods, suitable for big data era. Exploring the detailed plasma transport and heating mechanisms in near-Earth space with multi-point, in-situ measurements, provides a better understanding of the nature of plasma. This may therefore lead to progress also in laboratory plasma physics or different astrophysical plasma systems.

Acknowledgments
Work of KN and JJ were supported by NASA grant NNX17AI50G. Work of XM was supported by NASA grant NNX16AF89G.

References

Biskamp, D. (2000), *Magnetic Reconnection in Plasmas.*

Borgogno, D., F. Califano, M. Faganello, and F. Pegoraro (2015), Double-reconnected magnetic structures driven by kelvin-helmholtz vortices at the earth's magnetosphere, *Physics of Plasmas*, *22*(3), 032301, doi:http://dx.doi.org/10.1063/1.4913578.

Borovsky, J. E., and T. E. Cayton (2011), Entropy mapping of the outer electron radiation belt between the magnetotail and geosynchronous orbit, *Journal of Geophysical Research (Space Physics)*, *116*, A06216, doi:10.1029/2011JA016470.

Burch, J. L., T. E. Moore, R. B. Torbert, and B. L. Giles (2016), Magnetospheric Multiscale Overview and Science Objectives, *Space Science Reviews*, *199*, 5–21, doi:10.1007/s11214-015-0164-9.

Chandrasekhar, S. (1961), *Hydrodynamic and Hydromagnetic Stability*, Oxford Univ. Press, New York.

Chaston, C., J. Bonnell, J. P. McFadden, C. W. Carlson, C. Cully, O. Le Contel, A. Roux, H. U. Auster, K. H. Glassmeier, V. Angelopoulos, and C. T. Russell (2008), Turbulent heating and cross-field transport near the magnetopause from themis, *Geophysical Research Letters*, *35*(17), doi:10.1029/2008GL033601.

Chaston, C. C., T. D. Phan, J. W. Bonnell, F. S. Mozer, M. Acuńa, M. L. Goldstein, A. Balogh, M. Andre, H. Reme, and A. Fazakerley (2005), Drift-kinetic alfvén waves observed near a reconnection x line in the earth's magnetopause, *Phys. Rev. Lett.*, *95*, 065,002, doi:10.1103/PhysRevLett.95.065002.

Chaston, C. C., M. Wilber, F. S. Mozer, M. Fujimoto, M. L. Goldstein, M. Acuna, H. Reme, and A. Fazakerley (2007), Mode conversion and anomalous transport in kelvin-helmholtz vortices and kinetic alfvén waves at the earth's magnetopause, *Phys. Rev. Lett.*, *99*, 175,004, doi:10.1103/PhysRevLett.99.175004.

Chaston, C. C., C. W. Carlson, J. P. McFadden, R. E. Ergun, and R. J. Strangeway (2007a), How important are dispersive alfvÃ©n waves for auroral particle acceleration?, *Geophysical Research Letters*, *34*(7), doi:10.1029/2006GL029144.

Chaston, C. C., J. R. Johnson, M. Wilber, M. Acuna, M. L. Goldstein, and H. Reme (2009), Kinetic alfvén wave turbulence and transport through a reconnection diffusion region, *Phys. Rev. Lett.*, *102*, 015,001, doi:10.1103/PhysRevLett.102.015001.

Chaston, C. C., Y. Yao, N. Lin, C. Salem, and G. Ueno (2013), Ion heating by broadband electromagnetic waves in the magnetosheath and across the magnetopause, *Journal of Geophysical Research: Space Physics*, *118*(9), 5579–5591, doi:10.1002/jgra.50506.

Chaston, C. C., J. W. Bonnell, and C. Salem (2014), Heating of the plasma sheet by broadband electromagnetic waves, *Geophysical Research Letters*, *41*, 8185–8192, doi:10.1002/2014GL062116.

Chen, L., Z. Lin, and R. White (2001), On resonant heating below the cyclotron frequency, *Physics of Plasmas*, *8*, 4713–4716, doi:10.1063/1.1406939.

Chen, Q., A. Otto, and L. C. Lee (1997), Tearing instability, Kelvin-Helmholtz instability, and magnetic reconnection, *J. Geophys. Res.*, *102*, 151–161.

Cowee, M. M., D. Winske, and S. P. Gary (2009), Two-dimensional hybrid simulations of superdiffusion at the magnetopause driven by Kelvin-Helmholtz instability, *Journal of Geophysical Research (Space Physics)*, *114*, A10209, doi:10.1029/2009JA014222.

Dai, L., C. Wang, Y. Zhang, B. Lavraud, J. Burch, C. Pollock, and R. B. Torbert (2017), Kinetic alfvÃ©n wave explanation of the hall fields in magnetic reconnection, *Geophysical Research Letters*, *44*(2), 634–640, doi:10.1002/2016GL071044.

Delamere, P. A., R. J. Wilson, and A. Masters (2011), Kelvin-Helmholtz instability at Saturn's magnetopause: Hybrid simulations, *Journal of Geophysical Research (Space Physics)*, *116*, A10222, doi:10.1029/2011JA016724.

Delamere, P. A., B. Burkholder, and X. Ma (2018), Three-dimensional hybrid simulation of viscous-like processes at saturn's magnetopause boundary, *Geophysical Research Letters*, *0*(0), doi:10.1029/2018GL078922.

Dimmock, A. P., A. Osmane, T. I. Pulkkinen, and K. Nykyri (2015), A statistical study of the dawn-dusk asymmetry of ion temperature anisotropy and mirror mode occurrence in the terrestrial dayside magnetosheath using themis data, *Journal of Geophysical Research: Space Physics*, pp. n/a–n/a, doi:10.1002/2015JA021192, 2015JA021192.

Eriksson, S., B. Lavraud, F. D. Wilder, J. E. Stawarz, B. L. Giles, J. L. Burch, W. Baumjohann, R. E. Ergun, P.-A. Lindqvist, W. Magnes, C. J. Pollock, C. T. Russell, Y. Saito, R. J. Strangeway, R. B. Torbert, D. J. Gershman, Y. V. Khotyaintsev, J. C. Dorelli, S. J. Schwartz, L. Avanov, E. Grimes, Y. Vernisse, A. P. Sturner, T. D. Phan, G. T. Marklund, T. E. Moore, W. R. Paterson, and K. A. Goodrich (2016), Magnetospheric Multiscale observations of magnetic reconnection associated with Kelvin-Helmholtz waves, *Geophys. Res. Lett.*, *43*, 5606–5615, doi:10.1002/2016GL068783.

Faganello, M., F. Califano, F. Pegoraro, T. Andreussi, and S. Benkadda (2012), Magnetic reconnection and kelvin-helmholtz instabilities at the earth's magnetopause, *Plasma Physics and Controlled Fusion*, *54*(12), 124,037.

Fairfield, D. H., A. Otto, T. Mukai, S. Kokubun, R. P. Lepping, J. T. Steinberg, A. J. Lazarus, and T. Yamamoto (2000), Geotail observations of the Kelvin-Helmholtz instability at the eqatorial magnetotail boundary for parallel northward fields, *J. Geophys. Res.*, *105*, 21,159–21,174.

Fairfield, D. H., A. Otto, T. Mukai, S. Kokubun, R. P. Lepping, J. T. Steinberg, A. J. Lazarus, and T. Yamamoto (2000), Geotail observations of the Kelvin-Helmholtz instability at the equatorial magnetotail boundary for parallel northward fields, *Journal of Geophysical Research*, *105*, 21,159–21,174, doi:10.1029/1999JA000316.

Foullon, C., E. Verwichte, V. M. Nakariakov, K. Nykyri, and C. J. Farrugia (2011), Magnetic Kelvin-Helmholtz Instability at the Sun, *Astrophys. J. Lett.*, *729*, L8, doi:10.1088/2041-8205/729/1/L8.

Foullon, C., E. Verwichte, K. Nykyri, M. J. Aschwanden, and I. G. Hannah (2013), Kelvin-Helmholtz Instability of the CME Reconnection Outflow Layer in the Low Corona, *Astrophys. J.*, *767*, 170, doi:10.1088/0004-637X/767/2/170.

Fujimoto, M., and T. Terasawa (1994), Anomalous ion mixing within an MHD scale Kelvin-Helmholtz vortex, *J. Geophys. Res.*, *99*, 8601–8614.

Graham, D. B., Y. V. Khotyaintsev, C. Norgren, A. Vaivads, M. André, P.-A. Lindqvist, G. T. Marklund, R. E. Ergun, W. R. Paterson, D. J. Gershman, B. L. Giles, C. J. Pollock, J. C. Dorelli, L. A. Avanov, B. Lavraud, Y. Saito, W. Magnes, C. T. Russell, R. J. Strangeway, R. B. Torbert, and J. L. Burch (2016), Electron currents and heating in the ion diffusion region of asymmetric reconnection, *Geophysical Research Letters*, *43*(10), 4691–4700, doi:10.1002/2016GL068613.

Graham, D. B., Y. V. Khotyaintsev, C. Norgren, A. Vaivads, M. André, S. Toledo-Redondo, P.-A. Lindqvist, G. T. Marklund, R. E. Ergun, W. R. Paterson, D. J. Gershman, B. L. Giles, C. J. Pollock, J. C. Dorelli, L. A. Avanov, B. Lavraud, Y. Saito, W. Magnes, C. T. Russell, R. J. Strangeway, R. B. Torbert, and J. L. Burch (2017), Lower hybrid waves in the ion diffusion and magnetospheric inflow regions, *Journal of Geophysical Research: Space Physics*, *122*(1), 517–533, doi:10.1002/2016JA023572.

Hasegawa, A., and L. Chen (1976), Kinetic processes in plasma heating by resonant mode conversion of Alfvén wave, *Physics of Fluids*, *19*, 1924–1934, doi:10.1063/1.861427.

Hasegawa, A., and K. Mima (1978), Anomalous transport produced by kinetic alfvÃ©n wave turbulence, *Journal of Geophysical Research: Space Physics*, *83*(A3), 1117–1123, doi:10.1029/JA083iA03p01117.

Hasegawa, H., M. Fujimoto, T.-D. Phan, H. Reme, A. Balogh, M. W. Dunlop, C. Hashimoto, and R. TanDokoro (2004), Transport of solar wind into earth's magnetosphere through rolled-up Kelvin-Helmholtz vortices, *Nature*, *430*, 755–758.

Hasegawa, H., A. Retinò, A. Vaivads, Y. Khotyaintsev, M. André, T. K. M. Nakamura, W.-L. Teh, B. U. Ö. Sonnerup, S. J. Schwartz, Y. Seki, M. Fujimoto, Y. Saito, H. Rème, and P. Canu (2009), Kelvin-Helmholtz waves at the Earth's magnetopause: Multiscale development and associated reconnection, *Journal of Geophysical Research (Space Physics)*, *114*, A12207, doi:10.1029/2009JA014042.

Henry, Z. W., K. Nykyri, T. W. Moore, A. P. Dimmock, and X. Ma (2017), On the dawn-dusk asymmetry of the kelvin-helmholtz instability between 2007 and 2013, *Journal of Geophysical Research: Space Physics*, *122*(12), 11,888–11,900, doi:10.1002/2017JA024548.

Hietala, H., T. D. Phan, V. Angelopoulos, M. Oieroset, M. O. Archer, T. Karlsson, and F. Plaschke (2018), In situ observations of a magnetosheath high-speed jet triggering magnetopause reconnection, *Geophysical Research Letters*, *45*(4), 1732–1740, doi:10.1002/2017GL076525.

Hwang, K.-J., M. M. Kuznetsova, F. Sahraoui, M. L. Goldstein, E. Lee, and G. K. Parks (2011a), Kelvin-Helmholtz waves under southward interplanetary magnetic field, *Journal of Geophysical Research (Space Physics)*, *116*, A08210, doi:10.1029/2011JA016596.

Hwang, K.-J., M. M. Kuznetsova, F. Sahraoui, M. L. Goldstein, E. Lee, and G. K. Parks (2011b), Kelvin-Helmholtz waves under southward interplanetary magnetic field, *Journal of Geophysical Research*, *116*, A08210, doi:10.1029/2011JA016596.

Izutsu, T., H. Hasegawa, T. K. M. Nakamura, and M. Fujimoto (2012), Plasma transport induced by kinetic alfvÃ©n wave turbulence, *Physics of Plasmas*, *19*(10), 102,305, doi:10.1063/1.4759167.

Johnson, J., S. Wing, and P. Delamere (2014), Kelvin helmholtz instability in planetary magnetospheres, *Space Science Reviews*, *184*(1-4), 1–31, doi:10.1007/s11214-014-0085-z.

Johnson, J. R., and C. Z. Cheng (1997), Kinetic Alfvén waves and plasma transport at the magnetopause, *Geophysical Research Letters*, *24*, 1423–1426, doi:10.1029/97GL01333.

Johnson, J. R., and C. Z. Cheng (2001), Stochastic ion heating at the magnetopause due to kinetic Alfvén waves, *Geophysical Research Letters*, *28*(23), 4421–4424, doi:10.1029/2001GL013509.

Johnson, J. R., and S. Wing (2009a), Northward interplanetary magnetic field plasma sheet entropies, *Journal of Geophysical Research (Space Physics)*, *114*, A00D08, doi:10.1029/2008JA014017.

Johnson, J. R., and S. Wing (2009b), Northward interplanetary magnetic field plasma sheet entropies, *Journal of Geophysical Research: Space Physics*, *114*(A9), doi:10.1029/2008JA014017.

Karimabadi, H., V. Roytershteyn, H. X. Vu, Y. A. Omelchenko, J. Scudder, W. Daughton, A. Dimmock, K. Nykyri, M. Wan, D. Sibeck, M. Tatineni, A. Majumdar, B. Loring, and B. Geveci (2014), The link between shocks, turbulence, and magnetic reconnection in collisionless plasmas, *Physics of Plasmas*, *21*(6), 062308, doi:10.1063/1.4882875.

Kavosi, S., and J. Raeder (2015), Ubiquity of Kelvin-Helmholtz waves at Earth/'s magnetopause, *Nature Commun*, *6*, 7019, doi:doi:10.1038/ncomms8019.

Laitinen, T. V., Y. V. Khotyaintsev, M. André, A. Vaivads, and H. Rème (2010), Local influence of magnetosheath plasma beta fluctuations on magnetopause reconnection, *Annales Geophysicae*, *28*(5), 1053–1063, doi:10.5194/angeo-28-1053-2010.

Lee, L. C., J. R. Johnson, and Z. W. Ma (1994), Kinetic alfvÃ©n waves as a source of plasma transport at the dayside magnetopause, *Journal of Geophysical Research: Space Physics*, *99*(A9), 17,405–17,411, doi:10.1029/94JA01095.

Leroy, M. H. J., and R. Keppens (2017), On the influence of environmental parameters on mixing and reconnection caused by the Kelvin-Helmholtz instability at the magnetopause, *Physics of Plasmas*, *24*(1), 012,906, doi:10.1063/1.4974758.

Li, W., M. André, Y. V. Khotyaintsev, A. Vaivads, D. B. Graham, S. Toledo-Redondo, C. Norgren, P. Henri, C. Wang, B. B. Tang, B. Lavraud, Y. Vernisse, D. L. Turner, J. Burch, R. Torbert, W. Magnes, C. T. Russell, J. B. Blake, B. Mauk, B. Giles, C. Pollock, J. Fennell, A. Jaynes, L. A. Avanov, J. C. Dorelli, D. J. Gershman, W. R. Paterson, Y. Saito, and R. J. Strangeway (2016), Kinetic evidence of magnetic reconnection due to Kelvin-Helmholtz waves, *Geophys. Res. Lett.*, *43*, 5635–5643, doi:10.1002/2016GL069192.

Liang, J., Y. Lin, J. R. Johnson, X. Wang, and Z.-X. Wang (2016), Kinetic Alfvén waves in three-dimensional magnetic reconnection, *Journal of Geophysical Research (Space Physics)*, *121*, 6526–6548, doi:10.1002/2016JA022505.

Liang, J., Y. Lin, J. R. Johnson, Z.-X. Wang, and X. Wang (2017), Ion acceleration and heating by kinetic alfvÃ©n waves associated with magnetic reconnection, *Physics of Plasmas*, *24*(10), 102,110, doi:10.1063/1.4991978.

Lin, D., C. Wang, W. Li, B. Tang, X. Guo, and Z. Peng (2014), Properties of Kelvin-Helmholtz waves at the magnetopause under northward interplanetary magnetic field: Statistical study, *Journal of Geophysical Research (Space Physics)*, *119*, 7485–7494, doi:10.1002/2014JA020379.

Lin, Y., J. R. Johnson, and X. Wang (2012), Three-dimensional mode conversion associated with kinetic Alfvén waves, *Physical Review Letters*, *109*(12), 125003, doi:10.1103/PhysRevLett.109.125003.

Liu, Y.-H., M. Hesse, F. Guo, H. Li, and T. K. M. Nakamura (2018), Strongly localized magnetic reconnection by the super-Alfvénic shear flow, *Physics of Plasmas*, *25*(8), 080,701, doi:10.1063/1.5042539.

Ma, X., and A. Otto (2014), Nonadiabatic heating in magnetic reconnection, *Journal of Geophysical Research: Space Physics*, *119*(7), 5575–5588, doi:10.1002/2014JA019856.

Ma, X., A. Otto, and P. A. Delamere (2014a), Interaction of magnetic reconnection and Kelvin-Helmholtz modes for large magnetic shear: 1. Kelvin-Helmholtz trigger, *Journal of Geophysical Research: Space Physics*, *119*(2), 781–797, doi:10.1002/2013JA019224.

Ma, X., A. Otto, and P. A. Delamere (2014b), Interaction of magnetic reconnection and Kelvin-Helmholtz modes for large magnetic shear: 2. reconnection trigger, *Journal of Geophysical Research: Space Physics*, *119*(2), 808–820, doi:10.1002/2013JA019225.

Ma, X., A. Otto, and P. A. Delamere (2016), Magnetic reconnection with a fast perpendicular sheared flow, *Journal of Geophysical Research (Space Physics)*, *121*, 9427–9442, doi:10.1002/2016JA023107.

Ma, X., P. Delamere, A. Otto, and B. Burkholder (2017), Plasma transport driven by the three-dimensional kelvin-helmholtz instability, *Journal of Geophysical Research: Space Physics*, *122*(10), 10,382–10,395, doi:10.1002/2017JA024394.

Masson, A., and K. Nykyri (2018), Kelvin–helmholtz instability: Lessons learned and ways forward, *Space Science Reviews*, *214*(4), 71, doi:10.1007/s11214-018-0505-6.

Matsumoto, Y., and M. Hoshino (2004), Onset of turbulence induced by a Kelvin-Helmholtz vortex, *Geophys. Res. Lett.*, *31*, L02807, doi:10.1029/2003GL018195.

Matsumoto, Y., and M. Hoshino (2006), Turbulent mixing and transport of collisionless plasmas across a stratified velocity shear layer, *Journal of Geophysical Research (Space Physics)*, *111*, A05213, doi:10.1029/2004JA010988.

Matsumoto, Y., and K. Seki (2010), Formation of a broad plasma turbulent layer by forward and inverse energy cascades of the Kelvin-Helmholtz instability, *Journal of Geophysical Research (Space Physics)*, *115*, A10231, doi:10.1029/2009JA014637.

Miura, A. (1987), Simulation of Kelvin-Helmholtz instability at the magnetospheric boundary, *J. Geophys. Res.*, *92*, 3195–3206, doi:10.1029/JA092iA04p03195.

Miura, A. (1997), Compressible magnetohydrodynamic Kelvin-Helmholtz instability with vortex pairing in the two-dimensional transverse configuration, *Physics of Plasmas*, *4*, 2871–2885, doi:10.1063/1.872419.

Miura, A., and J. R. Kan (1992), Line-tying effects in the Kelvin-Helmholtz instability, *Geophysical Research Letters*, *19*, 1611–1614, doi:10.1029/92GL01448.

Miura, A., and P. L. Pritchett (1982), Nonlocal stability analysis of the MHD Kelvin-Helmholtz instability in a compressible plasma, *J. Geophys. Res.*, *87*, 7431–7444, doi:10.1029/JA087iA09p07431.

Moore, T. (2012), Identifying signatures of plasma waves and reconnection associated with kelvin-helmholtz activity, Ms thesis, Embry-Riddle Aeronautical University.

Moore, T. W., K. Nykyri, and A. P. Dimmock (2016), Cross-scale energy transport in space plasmas, *Nature Physics*, p. DOI:10.1038/NPHYS3869, doi:DOI:10.1038/NPHYS3869.

Moore, T. W., K. Nykyri, and A. P. Dimmock (2017), Ion-scale wave properties and enhanced ion heating across the low-latitude boundary layer during kelvin-helmholtz instability, *Journal of Geophysical Research: Space Physics*, *122*(11), 11,128–11,153, doi:10.1002/2017JA024591.

Nakamura, T. K., D. Hayashi, M. Fujimoto, and I. Shinohara (2004), Decay of MHD-Scale Kelvin-Helmholtz Vortices Mediated by Parasitic Electron Dynamics, *Physical Review Letters*, *92*(14), 145001, doi:10.1103/PhysRevLett.92.145001.

Nakamura, T. K. M., and W. Daughton (2014), Turbulent plasma transport across the Earth's low-latitude boundary layer, *Geophys. Res. Lett.*, *41*, 8704–8712, doi:10.1002/2014GL061952.

Nakamura, T. K. M., M. Fujimoto, and A. Otto (2006), Magnetic reconnection induced by weak kelvin-helmholtz instability and the formation of the low-latitude boundary layer, *Geophys. Res. Lett.*, *33*, L14,106, doi:10.1029/2006GL026318.

Nakamura, T. K. M., M. Fujimoto, and A. Otto (2008), Structure of an MHD-scale Kelvin-Helmholtz vortex: Two-dimensional two-fluid simulations including finite electron inertial effects, *Journal of Geophysical Research*, *113*, A09204, doi:10.1029/2007JA012803.

Nakamura, T. K. M., H. Hasegawa, I. Shinohara, and M. Fujimoto (2011), Evolution of an MHD-scale Kelvin-Helmholtz vortex accompanied by magnetic reconnection: Two-dimensional particle simulations, *Journal of Geophysical Research (Space Physics)*, *116*, A03227, doi:10.1029/2010JA016046.

Nakamura, T. K. M., H. Hasegawa, W. Daughton, S. Eriksson, W. Y. Li, and R. Nakamura (2017), Turbulent mass transfer caused by vortex induced reconnection in collisionless magnetospheric plasmas, *Nature Communications*, *8*(1), doi:10.1038/s41467-017-01579-0.

Nykyri, K. (2013), Impact of MHD shock physics on magnetosheath asymmetry and Kelvin-Helmholtz instability, *Journal of Geophysical Research (Space Physics)*, *118*, 5068–5081, doi:10.1002/jgra.50499.

Nykyri, K., and A. P. Dimmock (2016), Statistical study of the ULF Pc4-Pc5 range fluctuations in the vicinity of Earth's magnetopause and correlation with the Low Latitude Boundary Layer thickness, *Advances in Space Research*, *58*, 257–267, doi:10.1016/j.asr.2015.12.046.

Nykyri, K., and C. Foullon (2013), First magnetic seismology of the CME reconnection outflow layer in the low corona with 2.5-D MHD simulations of the Kelvin-Helmholtz instability, *Geophys. Res. Lett.*, *40*, 4154–4159, doi:10.1002/grl.50807.

Nykyri, K., and A. Otto (2001), Plasma transport at the magnetospheric boundary due to reconnection in Kelvin-Helmholtz vortices, *Geophys. Res. Lett.*, *28*, 3565–3568, doi:10.1029/2001GL013239.

Nykyri, K., and A. Otto (2004), Influence of the Hall term on KH instability and reconnection inside KH vortices, *Ann. Geophys.*, *22*, 935–949, doi:10.5194/angeo-22-935-2004.

Nykyri, K., A. Otto, B. Lavraud, C. Mouikis, L. Kistler, A. Balogh, and H. Réme (2006), Cluster observations of reconnection due to the Kelvin-Helmholtz instability at the dawn side magnetospheric flank, *Ann. Geophys.*, *24*, 2619–2643.

Nykyri, K., A. Otto, E. Adamson, E. Dougal, and J. Mumme (2011), Cluster observations of a cusp diamagnetic cavity: Structure, size, and dynamics, *Journal of Geophysical Research (Space Physics)*, *116*, A03228, doi:10.1029/2010JA015897.

Nykyri, K., A. Otto, E. Adamson, E. Kronberg, and P. Daly (2012), On the origin of high-energy particles in the cusp diamagnetic cavity, *Journal of Atmospheric and Solar-Terrestrial Physics*, *87*, 70–81, doi:10.1016/j.jastp.2011.08.012.

Nykyri, K., X. Ma, A. Dimmock, C. Foullon, A. Otto, and A. Osmane (2017), Influence of velocity fluctuations on the kelvin-helmholtz instability and its associated mass transport, *Journal of Geophysical Research: Space Physics*, *122*(9), 9489–9512, doi:10.1002/2017JA024374, 2017JA024374.

Nykyri, K., C. Chu, X. Ma, S. A. Fuselier, and R. Rice (2019), First mms observation of energetic particles trapped in high-latitude magnetic field depressions, *Journal of Geophysical Research: Space Physics*, *124*(1), 197–210, doi:10.1029/2018JA026131.

Otto, A., and D. H. Fairfield (2000), Kelvin-Helmholtz instability at the magnetotail boundary: MHD simulation and comparison with Geotail observations, *J. Geophys. Res.*, *105*, 21,175–21,190.

Rönnmark, K. (1982), Waves in homogenous, anisotropic multicomponent plasmas (WHAMP), *KRI*, *Tech. rep.*

Shay, M. A., J. F. Drake, J. P. Eastwood, and T. D. Phan (2011), Super-alfvénic propagation of substorm reconnection signatures and poynting flux, *Phys. Rev. Lett.*, *107*, 065,001.

Shi, F., Y. Lin, and X. Wang (2013), Global hybrid simulation of mode conversion at the dayside magnetopause, *Journal of Geophysical Research (Space Physics)*, *118*, 6176–6187, doi:10.1002/JournalofGeophysicalResearcha.50587.

Sonnerup, B. (1980), Theory of the low-latitude boundary layer, *Journal of Geophysical Research: Space Physics*, *85*(A5), 2017–2026, doi:10.1029/JA085iA05p02017.

Stasiewicz, K., P. Bellan, C. Chaston, C. Kletzing, R. Lysak, J. Maggs, O. Pokhotelov, C. Seyler, P. Shukla, L. Stenflo, A. Streltsov, and J.-E. Wahlund (2000), Small scale alfvénic structure in the aurora, *Space Science Reviews*, *92*, 423–533.

Stawarz, J. E., S. Eriksson, F. D. Wilder, R. E. Ergun, S. J. Schwartz, A. Pouquet, J. L. Burch, B. L. Giles, Y. Khotyaintsev, O. L. Contel, P.-A. Lindqvist, W. Magnes, C. J. Pollock, C. T. Russell, R. J. Strangeway, R. B. Torbert, L. A. Avanov, J. C. Dorelli, J. P. Eastwood, D. J. Gershman, K. A. Goodrich, D. M. Malaspina, G. T. Marklund, L. Mirioni, and A. P. Sturner (2016), Observations of turbulence in a Kelvin-Helmholtz event on 8 september 2015 by the Magnetospheric Multiscale mission, *Journal of Geophysical Research: Space Physics*, *121*(11), 11,021–11,034, doi:10.1002/2016JA023458, 2016JA023458.

Taroyan, Y., and R. Erdelyi (2002), Resonant and kelvin-helmholtz instabilities on the magnetopause, *Physics of Plasmas*, *9*(7), 3121–3129, doi:10.1063/1.1481746.

Taylor, M., and B. Lavraud (2008), Observation of three distinct ion populations at the kelvin-helmholtz-unstable magnetopause, *Ann. Geophys.*, *26*, 1559–1566.

Thomas, V. A., and D. Winske (1993), Kinetic simulations of the Kelvin-Helmholtz instability at the magnetopause, *J. Geophys. Res.*, *98*, 11,425–11,438.

Vaivads, A., A. Retinò, Y. V. Khotyaintsev, and M. André (2010), The alfvén edge in asymmetric reconnection, *Annales Geophysicae*, *28*(6), 1327–1331, doi:10.5194/angeo-28-1327-2010.

Vernisse, Y., B. Lavraud, S. Eriksson, D. J. Gershman, J. Dorelli, C. Pollock, B. Giles, N. Aunai, L. Avanov, J. Burch, M. Chandler, V. Coffey, J. Dargent, R. E. Ergun, C. J. Farrugia, V. Génot, D. B. Graham, H. Hasegawa, C. Jacquey, I. Kacem, Y. Khotyaintsev, W. Li, W. Magnes, A. Marchaudon, T. Moore, W. Paterson, E. Penou, T. D. Phan, A. Retino, C. T. Russell, Y. Saito, J.-A. Sauvaud, R. Torbert, F. D. Wilder, and S. Yokota (2016), Signatures of complex magnetic topologies from multiple reconnection sites induced by Kelvin-Helmholtz instability, *Journal of Geophysical Research: Space Physics*, *121*(10), 9926–9939, doi:10.1002/2016JA023051, 2016JA023051.

Walsh, B. M., E. G. Thomas, K.-J. Hwang, J. B. H. Baker, J. M. Ruohoniemi, and J. W. Bonnell (2015), Dense plasma and kelvin-helmholtz waves at earth's dayside magnetopause, *Journal of Geophysical Research: Space Physics*, pp. n/a–n/a, doi:10.1002/2015JA021014, 2015JA021014.

Wang, C.-P., M. Gkioulidou, L. R. Lyons, and V. Angelopoulos (2012), Spatial distributions of the ion to electron temperature ratio in the magnetosheath and plasma sheet, *Journal of Geophysical Research (Space Physics)*, *117*, 8215, doi:10.1029/2012JA017658.

Wang, C.-P., M. Gkioulidou, L. R. Lyons, and V. Angelopoulos (2012), Spatial distributions of the ion to electron temperature ratio in the magnetosheath and plasma sheet, *Journal of Geophysical Research: Space Physics*, *117*(A8), doi:10.1029/2012JA017658.

Wilber, M., and R. M. Winglee (1995), Dawn-dusk asymmetries in the low-latitude boundary layer arising from the Kelvin-Helmholtz instability: A particle simulation, *J. Geophys. Res.*, *100*, 1883–1898.

Wilder, F. D., R. E. Ergun, S. J. Schwartz, D. L. Newman, S. Eriksson, J. E. Stawarz, M. V. Goldman, K. A. Goodrich, D. J. Gershman, D. M. Malaspina, J. C. Holmes, A. P. Sturner, J. L. Burch, R. B. Torbert, P.-A. Lindqvist, G. T. Marklund, Y. Khotyaintsev, R. J. Strangeway, C. T. Russell, C. J. Pollock, B. L. Giles, J. C. Dorrelli, L. A. Avanov, W. R. Patterson, F. Plaschke, and W. Magnes (2016), Observations of large-amplitude, parallel, electrostatic waves associated with the kelvin-helmholtz instability by the magnetospheric multiscale mission, *Geophysical Research Letters*, *43*(17), 8859–8866, doi:10.1002/2016GL070404.

Winant, C. D., and F. K. Browand (1974), Vortex pairing: the mechanism of turbulent mixing-layer growth at moderate Reynolds number, *Journal of Fluid Mechanics*, *63*, 237–255, doi:10.1017/S0022112074001121.

Wing, S., J. R. Johnson, P. T. Newell, and C.-I. Meng (2005), Dawn-dusk asymmetries, ion spectra, and sources in the northward interplanetary magnetic field plasma sheet, *Journal of Geophysical Research (Space Physics)*, *110*, A08205, doi:10.1029/2005JA011086.

Yan, G. Q., F. S. Mozer, C. Shen, T. Chen, G. K. Parks, C. L. Cai, and J. P. McFadden (2014), Kelvin-Helmholtz vortices observed by THEMIS at the duskside of the magnetopause under southward interplanetary magnetic field, *Geophys. Res. Lett.*, *41*, 4427–4434, doi:10.1002/2014GL060589.

Yan, G. Q., F. S. Mozer, C. Shen, T. Chen, G. K. Parks, C. L. Cai, and J. P. McFadden (2014), Kelvin-helmholtz vortices observed by themis at the duskside of the magnetopause under southward interplanetary magnetic field, *Geophysical Research Letters*, *41*(13), 4427–4434, doi:10.1002/2014GL060589, 2014GL060589.

Yao, Y., C. C. Chaston, K.-H. Glassmeier, and V. Angelopoulos (2011), Electromagnetic waves on ion gyro-radii scales across the magnetopause, *Geophysical Research Letters*, *38*(9), doi:10.1029/2011GL047328.